PREPRINT

Operator Theory: Advances and Applications

Unravelling topological determinants of excitable dynamics on graphs using analytical mean-field approaches

Marc-Thorsten Hütt and Annick Lesne

Abstract. We present our use of analytical mean-field approaches in investigating how the interplay between graph topology and excitable dynamics produce spatio-temporal patterns. We first detail the derivation of mean-field equations for a few simple model situations, mainly 3-state discrete-time excitable dynamics with an absolute or a relative excitation threshold. Comparison with direct numerical simulation shows that their solution satisfactorily predicts the steady-state excitation density. In contrast, they often fail to capture more complex dynamical features, however we argue that the analysis of this failure is in itself insightful, by pinpointing the key role of mechanisms neglected in the mean-field approach. Moreover, we show how second-order mean-field approaches, in which a topological object (e.g. a cycle or a hub) is considered as embedded in a mean-field surrounding, allow us to go beyond the spatial homogenization currently associated with plain mean-field calculations. The confrontation between these refined analytical predictions and simulation quantitatively evidences the specific contribution of this topological object to the dynamics.

Mathematics Subject Classification (2010). Primary 05C82; Secondary 92C42.

Keywords. Network dynamics, analytical approaches, simulation.

1. Introduction

The original mean-field approach has been introduced in statistical physics for the analysis of ferromagnetism [28]. Its insight is to approximately describe the effect of specific couplings between a given atom and its neighbors (actually all reduced to their spin) as the influence of their average magnetization,

This work has been completed in the framework of the ZiF programme *Discrete and continuous models in the theory of networks.*

acting as an homogeneous external magnetic field (the *mean field*). It has lead to a general class of methods, involving similar 'mean-field' ansatzes [19, 20]. In the context of dynamics on graphs, it has for example been applied to self-organized criticality [8], reaction-diffusion processes on networks for one-component [7] and multi-component systems [27], voter model [26], or excitable dynamics [6, 17, 18]. A general discussion of the accuracy of such methods can be found in [14] and the monograph [2]. The forest-fire model in [15] is the first attempt to take into account graph topology in a mean-field approach, via shortcut density.

In all dynamic models where nodes of the graph can be in a finite number of states, the general spirit of mean-field approaches is a space-implicit description in terms of the probability (in physical terms, the density) of each state. Such approaches provide an average view over space, initial conditions and stochasticity of the dynamics, based on ignoring spatial correlations and inhomogeneities. The validity of mean-field approximations thus requires weak correlations and statistical homogeneity. While standard mean-field approaches in continuous systems are shown to be valid above a critical dimension d_c, the situation is different on a graph, where mean-field failure is presumed to originate in the inherent heterogeneities of its topology and the way they influence the dynamics. In the context of processes on graphs, mean-field equations are usually not derived bottom-up from a microscopic stochastic description, but rather proposed straightforwardly in view of the qualitative features of the local dynamics, e.g. how many excited neighbors are required to excite a node in case of excitable dynamics [4, 25, 3, 24].

We will present in Section 2 the derivation of mean-field equations for two instances of discrete-time excitable dynamics on graphs. In both models, a node i of the graph can be either susceptible S, excited E, or refractory R. The dynamics is defined as a 3-state cellular automaton $S \to E \to R \to S$ according to the following rules: an excited node at time t becomes refractory at time $t+1$, a refractory node at time t becomes susceptible at time $t+1$ with a recovery probability p (else it remains refractory), and a susceptible node becomes excited according to the state at time t of the neighboring nodes on the graph. For the *absolute threshold model*, a susceptible node at time t becomes excited at time $t+1$ if it has at least q excited neighbors (we will mostly consider the simplest case $q = 1$), while for the *relative threshold model*, a susceptible node becomes excited at time $t+1$ if at least a fraction κ of its neighbors are excited at time t. Additionally, spontaneous excitations can occur at susceptible nodes with probability f per time step. When $p < 1$ (stochastic recovery) and/or $f > 0$ (spontaneous excitations), the dynamics is stochastic. An additional level of stochasticity comes from the randomness of initial conditions. What thus makes sense is to describe average behaviors. These two models are reminiscent of SIS and SIR models [16, 4], however no simple mapping can be drawn (excitation propagation is a stochastic step in SIS and SIR, involving a transmission probability), and their behaviors

differ. As for the underlying graphs, we actually consider *ensembles of graphs* defined by current models, from Erdős-Rényi random graphs [10] to Barabási-Albert scale-free graphs [1] to Molloy-Reed configuration model that samples graphs with any prescribed degree distribution, to hierarchical or modular complex networks [5].

To evaluate the validity of a mean-field approach and its limits, we have compared in Section 3 the analytical mean-field predictions and the numerical implementation of our two models of excitable dynamics on graphs. Failure of a mean-field approach means that either correlations between the nodes, or local network features, or both, matter. We will discuss the insights than can be gained from the analysis of this failure. Section 4 is devoted to the analytical strategies we have devised to go beyond basic mean-field approaches and take into account some specific topological features of the graph, in order to gain some general understanding of the interplay between graph topology and its excitable dynamics.

2. Mean-field equations for excitable dynamics on graphs

2.1. Principle of mean-field approximation(s)

Denoting $x_i(t)$ the state of node i at discrete time t, the standard mean-field approach for describing the average graph dynamics actually comprises two different approximations, whatever the considered model of dynamics. The first one is a *spatial de-correlation* of the node states when computing statistical averages: $\langle x_i(t)x_j(t)\rangle \approx \langle x_i(t)\rangle\langle x_j(t)\rangle$. The second one is a *spatial homogenization*, considering that $\langle x_i(t)\rangle$ is independent of the node i. These two approximations will allow us to derive autonomous, deterministic and space-implicit equations for the densities $c_\alpha(t) = \mathrm{Prob}[x_i(t) = \alpha]$, with here $\alpha = E, S, R$.

2.2. Absolute threshold $q = 1$ for excitation propagation

Mean-field dynamics is derived by identifying the probability that a given neighbor is not excited with the average and node-independent quantity $1 - c_E(t)$. A decorrelation approximation lies in considering an average quantity, while its node-independence amounts to an homogenization. Another homogenization arises in replacing the number of direct neighbors of a node (that is, its degree) with the average degree $\langle k\rangle$. This latter approximation is applied in particular to the probability that a node has at least an excited neighbor at time t, which is the condition for its excitation by neighbors in the absolute-threshold model. This probability is accordingly estimated as $1 - B(0, \langle k\rangle, c_E(t))$, where the binomial distribution can be explicitly expressed $B(0, \langle k\rangle, c_E(t)) = (1 - c_E(t))^{\langle k\rangle}$. This probability has then to be multiplied by $(1 - f)$ (no overriding spontaneous excitation) and by the homogenized probability $c_S(t)$ that the node is susceptible. Overall, mean-field

evolution equations for the state densities are:

$$\begin{cases} c_E(t+1) = c_S(t)\left[f + (1-f)[1-(1-c_E(t))^{\langle k\rangle}]\right] \\ c_R(t+1) = c_E(t) + (1-p)c_R(t) \\ c_S(t+1) = 1 - c_E(t+1) - c_R(t+1) \end{cases} \tag{2.1}$$

In the regimes where $c_E(t) \ll 1$, the term $1-(1-c_E(t))^{\langle k\rangle}$ simply reduces to $\langle k\rangle\, c_E(t)$. Note that the average degree $\langle k\rangle$ is usually not an integer: while the probabilistic reasoning makes sense only for integral $\langle k\rangle$, the resulting formula can be interpolated and extended to any real value of $\langle k\rangle$.

Fixed points of (2.1), i.e. $c_\alpha(t+1) = c_\alpha(t) = c^*_\alpha$ for $\alpha = E, S, R$, correspond to steady states. For all mean-field fixed points, we have: $p\, c^*_R = c^*_E$, $p(1-c^*_S) = c^*_E(1+p)$, whatever the excitation probability model and the value of f. For $f = 0$, there is a trivial (unstable) fixed point ($c^o_E = 0, c^o_R = 0, c^o_S = 1$) whatever the value of p. Still for $f = 0$, there is also a non trivial fixed point:

$$c^*_E = \frac{p\,(\langle k\rangle - 1)}{\langle k\rangle(p+1)}, \qquad c^*_S = \frac{1}{\langle k\rangle}, \qquad c^*_R = \frac{\langle k\rangle - 1}{\langle k\rangle(p+1)} \tag{2.2}$$

provided the consistency condition $\langle k\rangle c^*_E \ll 1$ holds. Else we have to solve numerically the non-linear equation:

$$c^*_E = [1 - c^*_E(1+1/p)]\left[f + (1-f)[1-(1-c^*_E)^{\langle k\rangle}]\right] \tag{2.3}$$

2.3. Relative threshold κ for excitation propagation

In case of a relative excitation threshold κ, the most basic mean-field approximation states that a susceptible node of degree k gets excited if its average number of excited neighbors, kc_E, is larger than $k\kappa$, that is if $c_E \geq \kappa$ whatever the node degree k. This leads to the simple evolution equations, where H is the Heaviside function:

$$\begin{cases} c_E(t+1) = c_S(t)\,[f \;+\; (1-f)H[c_E(t) - \kappa]] \\ c_R(t+1) = c_E(t) + (1-p)c_R(t) \\ c_S(t+1) = 1 - c_E(t+1) - c_R(t+1) \end{cases} \tag{2.4}$$

A refined set of equations can be obtained using combinatoric probabilistic arguments, and considering for all nodes the same homogenized degree, equal to the average degree $\langle k\rangle$. We define $\bar{n}_\kappa$ as the smallest integer larger or equal to $\kappa\langle k\rangle$, that is, $\bar{n}_\kappa = \lceil \kappa\,\langle k\rangle \rceil$. Excitation propagation at a susceptible node then requires that it has at least $\bar{n}_\kappa$ excited neighbors, whatever its actual degree. The mean-field evolution equations for a relative excitation threshold κ then coincide with those obtained for an absolute excitable threshold $q = \bar{n}_\kappa$. The factor $[1-(1-c_E(t))^{\langle k\rangle}]$ in the above mean-field evolution equations (2.1) is now to be replaced with:

$$\sum_{j=0}^{\lceil\langle k\rangle\rceil - \bar{n}_\kappa} \left(\begin{array}{c} \lceil\langle k\rangle\rceil \\ \bar{n}_\kappa + j \end{array} \right) c_E(t)^{\bar{n}_\kappa + j}(1-c_E(t))^{\lceil\langle k\rangle\rceil - \bar{n}_\kappa - j} \tag{2.5}$$

Note that $\langle k\rangle$ is usually not an integer, and has to be replaced by $\lceil\langle k\rangle\rceil$ for the binomial coefficient to make sense. For $\kappa \to 0$, we have $\bar{n}_\kappa = 1$, and the mean-field equations for an absolute threshold $q = 1$ are satisfactorily recovered. Overall, we obtain the coupled equations:

$$\begin{cases} c_E(t+1) &= f c_S(t) \\ &\quad +(1-f)c_S(t)\sum_{j=0}^{\lceil\langle k\rangle\rceil-\bar{n}_\kappa}\binom{\lceil\langle k\rangle\rceil}{\bar{n}_\kappa+j} c_E(t)^{\bar{n}_\kappa+j}(1-c_E(t))^{\lceil\langle k\rangle\rceil-\bar{n}_\kappa-j} \\ c_R(t+1) = c_E(t) + (1-p)c_R(t) \\ c_S(t+1) = 1 - c_E(t+1) - c_R(t+1) \end{cases} \tag{2.6}$$

When $c_E(t) \ll 1$, the term for $j = 0$ dominates and the above sum can be replaced in the numerical implementation by the proxy:

$$\binom{\lceil\langle k\rangle\rceil}{\bar{n}_\kappa} c_E(t)^{\bar{n}_\kappa} \tag{2.7}$$

For $f = 0$, the evolution described by the simple equations (2.4) has a non trivial stable fixed point:

$$c_E^* = \frac{p}{2p+1}, \qquad c_S^* = \frac{p}{2p+1}, \qquad c_R^* = \frac{1}{2p+1} \tag{2.8}$$

provided $\kappa < c_E^*$, i.e. $\kappa < p/(2p+1)$. When $\kappa > p/(2p+1)$, the stable fixed point becomes: $c_E^* = 0$, $c_S^* = 1$, $c_R^* = 0$. When the evolution is described by the refined mean-field equations (2.6) with the simplification (2.7), the fixed points in the absence of spontaneous excitations ($f = 0$) correspond to the solutions of:

$$c_E^* = \binom{\lceil\langle k\rangle\rceil}{\bar{n}_\kappa} (c_E^*)^{\bar{n}_\kappa}(1 - c_E^*(1+1/p)) \tag{2.9}$$

satisfying he condition $0 \le c_E^* \le p/(p+1)$, so that $c_R^* \ge 0$ and $c_S^* \ge 0$. This yields a trivial fixed point ($c_E^o = 0, c_R^o = 0, c_S^o = 1$) whatever the value of p. This fixed point is stable for $\bar{n}_\kappa \ge 2$ (the stability analysis is easily done by reducing the evolution to two coupled equations, e.g. for $c_E(t)$ and $c_R(t)$, and determining for which values of κ the eigenvalues of the Jacobian matrix have a modulus strictly lower than 1). For $\bar{n}_\kappa = 1$, i.e. for $\kappa < 1/\langle k\rangle$, the stable fixed point is associated to the nontrivial solution of (2.9).

For $f > 0$, we have to numerically solve the fixed point equations. However, at small f, a simple approximation is to identify the average excitation density with $c_E^o = f$ (instead of $c_E^o = 0$) at large values of κ, while the non trivial value c_E^* at low values of κ is considered to be unaffected by a small rate of spontaneous excitations. The good accuracy of these various analytical predictions for the steady-state excitation density is presented below n Section 3 and associated figures.

2.4. Evolution for degree classes

In the basic mean-field equations (2.1) and (2.6), graph topology is involved only through the average degree $\langle k\rangle$. It is possible to better take into account a broad degree distribution by considering degree classes, that is, subsets of

nodes of a given degree. We denote $c_E(k,t)$ the average excitation density of nodes of degree k (and similarly $c_S(k,t)$ and $c_R(k,t)$, for susceptible and refractory states). In the mean-field approximation for an excitable dynamics with absolute threshold $q = 1$, a node in the class of degree k has $k\,c_E(t)$ excited neighbors and a probability $1-(1-c_E(t)]^k$ to have at least one excited neighbor: some node heterogeneity is now included in the mean-field dynamics. Evolution equations become:

$$\left\{\begin{array}{ll} c_E(k,t+1) & = c_S(k,t)\left[f+(1-f)\left[1-(1-c_E(t)\right]^k\right] \\ c_R(k,t+1) & = c_k E(k,t)+(1-p)c_R(k,t) \\ c_S(k,t+1) & = 1-c_E(k,t+1)-c_R(k,t+1) \end{array}\right. \tag{2.10}$$

The overall excitation density is related to these partial densities by the relation $\sum_k \rho(k)\, c_E(k,t) = c_E(t)$ directly involving the degree distribution $\rho(k)$. However, several mean-field approximations are still present: at the dynamic level, we still ignore correlations between the states of the nodes, and at the network level, we neglect degree-degree correlations and consider the degree-average state for neighboring nodes.

In case of excitable dynamics with a relative threshold κ, we introduce $n_\kappa(k)$ as the smallest integer larger or equal to κk. The equation for $c_E(k,t)$ is the same as for an absolute threshold $q = n_\kappa(k)$:

$$c_E(k,t+1) = f\; c_S(k,t) + (1-f)\; c_S(k,t) \sum_{j=n_\kappa(k)}^{k} \left(\begin{array}{c} k \\ j \end{array} \right) c_E(t)^j (1-c_E(t))^{k-j} \tag{2.11}$$

In a finite graph (hence having a bounded maximal degree), equations for an absolute threshold $q = 1$ are recovered in the limit $\kappa \to 0$, when all $n_\kappa(k)$ reduce to 1.

A refinement is to take into account degree-degree correlations (see e.g. [23, 4] for application to SIS epidemic model and [27] for application to diffusion-annihilation process). An analysis of mean-field validity in the case where degree-degree correlations cannot be ignored is presented in [14], suggesting that the mean first-neighbor degree d is a good predictor of the validity (the more reliable the larger d); d reduces to the average degree $\langle k \rangle$ in uncorrelated networks. Degree-degree correlations are described by the conditional probability $\rho(k'|k)$ that the degree of a neighbor of a node of degree k is k'. For an excitable model with absolute threshold $q = 1$, the probability for a node of degree k to have at least an excited neighbor becomes $1-(1-\sum_{k'} \rho(k'|k)\; c_E(k',t))^k$, replacing $1-(1-c_E(t))^k$ in (2.10). The mean excitation field of a node, $\sum_{k'} \rho(k'|k)\; c_E(k',t) \equiv c_E(\mathrm{nn}(k),t)$, now depends on the node degree k. This modification of $c_E(t)$ into a degree-dependent local field $c_E(\mathrm{nn}(k),t)$ also holds in (2.11) for the model with a relative excitation threshold κ.

2.5. Pair-correlation equations

Identifying the probability that two neighboring nodes are simultaneously excited with $[c_E(t)]^2$ is often too crude. This approximation can be circumvented by introducing a quantity $c_{E,E}(t)$, describing the probability that two neighbors are simultaneously excited, and similar quantities for the other pair correlations [9, 22]. The evolution of state densities $c_\alpha(t)$ can be written in a less approximate way by involving these additional variables. For an excitable model with an absolute threshold $q = 1$, it comes:

$$c_E(t+1) = f c_S(t) + (1-f) c_S(t) \left[1 - \left(1 - \frac{c_{E,S}(t)}{c_S(t)} \right)^{\langle k \rangle} \right] \quad (2.12)$$

$$c_R(t+1) = c_E(t) + (1-p) c_R(t) \quad (2.13)$$

$$c_S(t+1) = 1 - c_E(t+1) - c_R(t+1) \quad (2.14)$$

While spatial homogenization remains, the mean-field decorrelation approximation is relaxed and displaced at a higher order, in a closure relation of the form $\langle xxyy \rangle = \langle xx \rangle \langle yy \rangle$ required to get an autonomous set of equations of evolution for the pair-correlations, as follows:

$$\begin{aligned} c_{E,S}(t+1) = \; & fp\, c_{S,R}(t) + (1-f)p\, \frac{c_{S,R}(t) c_{E,S}(t)}{c_S(t)} \\ & + (1-f) f c_{S,S}(t) \left(1 - \frac{c_{E,S}(t)}{c_S(t)} \right)^{\langle k \rangle - 1} \\ & + (1-f)^2 c_{S,S}(t) \left(1 - \frac{c_{E,S}(t)}{c_S(t)} \right)^{\langle k \rangle - 1} \left[1 - \left(1 - \frac{c_{E,S}(t)}{c_S(t)} \right)^{\langle k \rangle - 1} \right] \end{aligned} \quad (2.15)$$

This evolution equation for $c(E, S, t)$ contains four terms: the probability that in a pair of neighbors (S, R), the first one gets spontaneously excited and the second one recovers; the probability that in a pair of neighbors (S, S), the first one gets excited due to its excited neighbors and the second one recovers; the probability that in a pair of neighbors (S, S), the first one gets spontaneously excited and the second one escapes both spontaneous and neighbor-induced excitation and remains susceptible; the probability that in a pair of neighbors (S, S), the first one gets excited due to its excited neighbors and the second one escapes both spontaneous and neighbor-induced excitation and remains susceptible. Similar equations can be written for the other joint densities $c_{E,R}$

and $c_{S,R}$:

$$c_{E,R}(t+1) = c_{S,R}(t)\left[(1-p)f + (1-p)(1-f)\left[1-\left(1-\frac{c_{E,S}(t)}{c_S(t)}\right)^{\langle k\rangle}\right]\right] + c_{E,S}(t)\left[(f+(1-f)\left[1-\left(1-\frac{c_{E,S}(t)}{c_S(t)}\right)^{\langle k\rangle}\right]\right] \quad (2.16)$$

$$c_{S,R}(t+1) = c_{S,R}(t)\,(1-p)(1-f)\left(1-\frac{c_{E,S}(t)}{c_S(t)}\right)^{\langle k\rangle} + (1-p)p\,c_{R,R}(t) + p\,c_{E,R}(t) + (1-f)\,c_{E,S}(t)\left(1-\frac{c_{E,S}(t)}{c_S(t)}\right)^{\langle k\rangle} \quad (2.17)$$

supplemented with $c_S(t+1) = 1 - c_E(t+1) - c_R(t+1)$, $c_{S,S}(t+1) = c_S(t+1) - c_{S,E}(t+1) - c_{S,R}(t+1)$ and similar relationships for $c_{E,E}(t+1)$ and $c_{R,R}(t+1)$. Such pair-correlation equations have been used for instance to investigate co-activation and pinpoint its topological determinants, through a comparison of analytical predictions and numerical simulations [17].

3. Successes and failures of mean-field approaches: numerical checks

3.1. A remarkable power to predict excitation density in random graphs

An implicit step in the practical use of mean-field approaches is to identify empirical space averages that can be measured in experiments and simulation, with the statistical averages $c_\alpha(t)$ involved in the equations (here $\alpha = E, S, R$). The validity of this identification directly follows from the applicability of the law of large numbers, which has the same conditions of validity as the mean-field approximations, namely it also requires weak correlations and statistical homogeneity.

To evaluate the validity of mean-field approximations, we implemented numerically the two models of excitable dynamics on graph described in the introduction. They are specially suitable for a numerical analysis, since they actually take the form of three-state cellular automata. The initial condition is generally taken at random, with equal fractions of susceptible, excited and refractory nodes spanning the graph. All the spatio-temporal correlations and network heterogeneities are by construction taken into account in the simulation. We compared the steady-state mean-field excitation density c_E^* predicted analytically and its numerical value, observed in the simulation after discarding initial transients and performing a suitable time average.

As seen on Fig. 1, for excitable dynamics on a highly connected random graph (Erdős-Rényi graph of average degree 10), the simulated time-average excitation density lies around the mean-field prediction, with some fluctuations of relatively low amplitude. The goodness of the basic mean-field

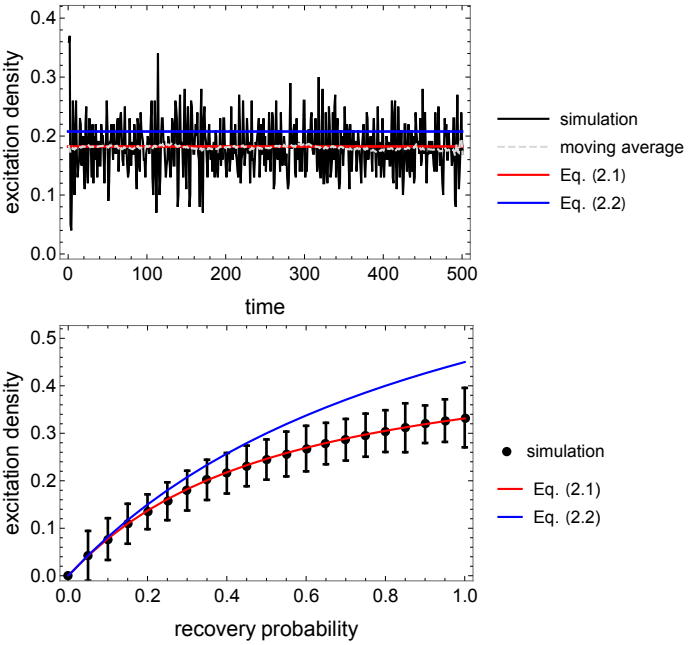

FIGURE 1. **Mean-field excitation density and its simulated counterpart on a highly connected random graph, for an absolute excitation threshold $q = 1$.** Simulation has been performed with a spontaneous excitation rate $f = 0.01$, on a random graph (Erdős-Rényi) with 100 nodes and 500 links. The upper panel displays a simulated trajectory for a recovery probability $p = 0.3$ (highly fluctuating black line), its moving average (light grey dashes), the approximate fixed point given by (2.2) and the steady-state solution of mean-field equations (2.1). The lower panel compares the excitation density obtained in the simulation, the fixed point (2.2) and the steady-state solution of (2.1) for varying values of the recovery probability p. Error bars on simulation points have been obtained from the last 250 time steps of a 500 time-step simulation starting from random initial conditions.

approach on highly connected random graphs relies (i) on the spatial homogeneity of these graphs, (ii) the fact that they are locally similar to a tree, and (iii) the large enough number of neighbors. Consequently it is respectively valid (i) to identify the node degrees with the average degree, (ii) to consider that there is no correlations between the states of node neighbors as if the topology around each node were star-like, and (iii) to identify the

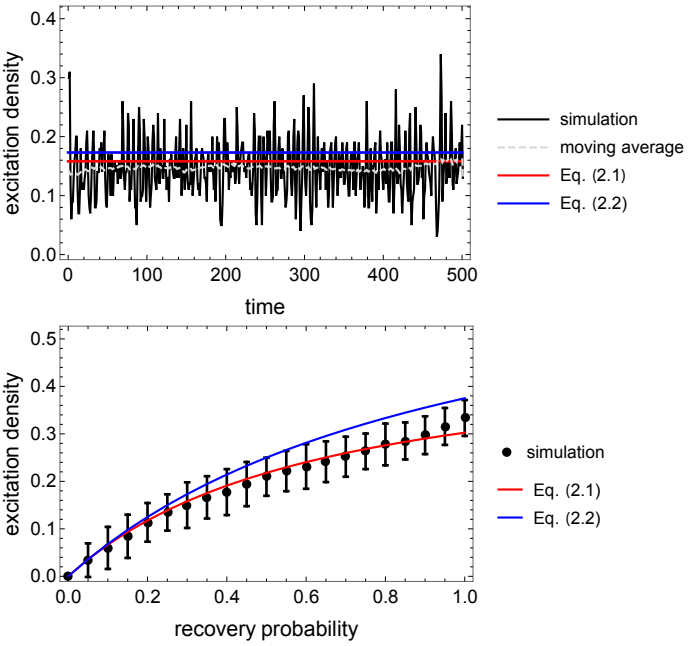

FIGURE 2. **Mean-field excitation density and its simulated counterpart on a low-connectivity random graph, for an absolute excitation threshold** $q = 1$**.** Same as Fig. 1 now on a random graph (Erdős-Rényi) with 100 nodes and 200 links.

excitation probability of the neighbors of a given node with the average excitation density. When the graph connectivity decreases, the prediction quality decreases, as seen on Fig. 2.

Considering scale-free graphs yields a prediction quality similar to that observed for low-connectivity random graph, as seen on Fig. 3. However, a marked difference is the range and nature of fluctuations, which now exhibit spikes. This latter feature is presumably due to the spatial heterogeneity of the network, where nodes of both small and high degree are present, and the fact that high-degree nodes may nucleate coherent waves of activation (see below, § 4.3 and [17]).

In the case of a relative excitation threshold, Fig. 4 shows the good agreement of both the mean-field prediction (2.8) and the stationary solution of mean-field equations (2.6) and (2.7) with the numerical steady-state. Both correctly predicts the exchange of stability between the non-trivial fixed point and the value $c_E^o = f$ corresponding to the extinction of excitation propagation. We have shown in [11] that a sustained activity (corresponding to the non trivial steady state) occurs up to a value κ_m that can be roughly estimated from the graph topology as the maximal degree k_{max} of the graph,

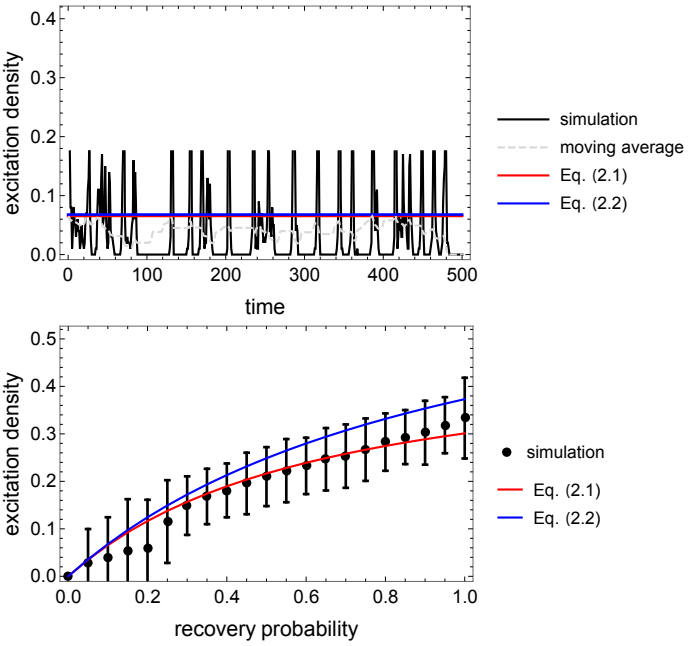

FIGURE 3. **Mean-field excitation density and its simulated counterpart on a scale-free graph for an absolute excitable threshold $q = 1$.** Same as Fig. 2 now on a a scale-free graph (Barabási-Albert) with 100 nodes and 197 links (corresponding to $m = 2$ links being added per node during preferential attachment).

in agreement with the upper bound $1/\langle k \rangle$ (larger that $1/k_{max}$) predicted here using mean-field analysis. The observed lower bound c_E^* can be explained as a fluctuation effect: the actual number of excited neighbors of a node of degree k can be higher than kc_E^*, which accommodates excitation propagation for relative threshold values higher than $\kappa = c_E^*$.

3.2. Insightful failures

Numerical simulations, Fig. 3, show that basic mean-field equations fail to describe the full complexity of excitable dynamics on graphs with a very broad degree distribution. They miss self-organized formation of coherent patterns of excitation, responsible of the spikes apparent on the time evolution of the overall excitation density. In showing the limits of considering the same average degree for all nodes, they indirectly demonstrate the central role of hubs in the dynamics of scale-free graphs. Actually, a sounder approximation is to consider that hubs act as organizing centers of the excitable dynamics, see § 4.3. An another numerical observation is the fact that plain mean-field description accounts for the excitation density but not at all for the

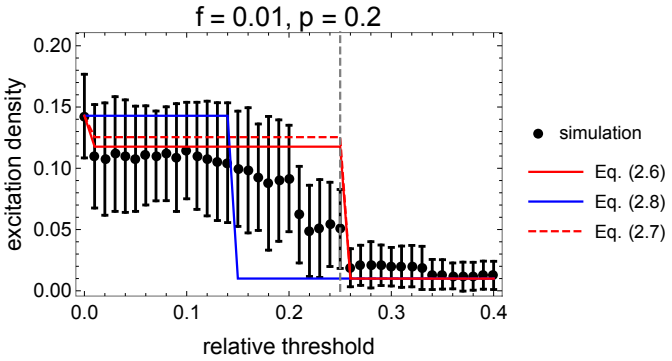

FIGURE 4. **Mean-field excitation density and its simulated counterpart on a random graph, in case of relative excitation threshold.** Simulation has been performed with a recovery probability $p = 0.2$, a spontaneous excitation rate $f = 0.01$, on a random graph (Erdős-Rényi) with 100 nodes and 200 links. The time-averaged excitation density obtained in the simulation (black dots) is compared for various values of the relative threshold κ with the fixed point (2.8) and the steady-state solution of mean-field equations (2.6) and (2.7). Error bars on simulation points have been obtained from the last 250 time steps of a 500 time-step simulation starting from random initial conditions. The first step (blue line, eq. (2.8)) is located at $\kappa = p/(2p+1)$ and the second step (red continuous and dashed lines, eqs. (2.6) and (2.7)) is at the higher value $\kappa = 1/\langle k \rangle$, indicated by the gray dashed vertical line.

correlation between co-activation patterns and graph topology [21]. Finally, mean-field equations provide an average view of the dynamics: they do not reflect dynamical features of individual trajectories.

Mean-field analysis alone is not reliable enough to grasp understanding of dynamics on complex networks. In general there is no internal way to delineate which results are correct and which are by far different from the actual behavior. On the other hand, numerical simulation alone is often as complex and intricate as an experiment on the real system, and it may prove difficult to dissect and identify the local features and basic mechanisms responsible of the observed behavior. We claim that a reliable understanding can be gained by the conjunction of mean-field analysis and numerical simulation.

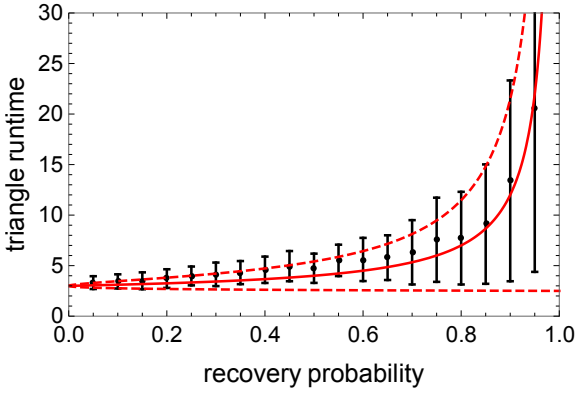

FIGURE 5. **Cycling excitation in a triangle.** Considering the runtime of an excitation in a triangle, with initial condition (E, S, R), the figure compares the analytical prediction $\tau(L,p) = L - 1 + \tau_{break}(L,p)$ for $L = 3$, with $\tau_{break}(L,p)$ given in (4.1), continuous red line, plus/minus the corresponding standard deviation $\sqrt{p/(1-p)^2}$, dashed red lines, with the simulation result (black dots). Errors bars on the numerical estimates have been computed with 100 runs.

4. Second-order mean-field approach for topological devices

4.1. Principle

Mean-field approaches described above all involved a spatial homogenization over the nodes (or subsets of nodes) of the graph. This is obviously a critical gap for investigating the interplay between graph topology and excitable dynamics. To circumvent this gap, we devised a refined analytical approach involving a more detailed account of the topology. The contribution of a specific topological motif (for instance a triangle, a cycle, a shell of nodes at the same distance from a given hub, a module) to the overall dynamical behavior can be computed by considering it as a device embedded in a surrounding described by mean-field densities. This approach amounts to use a second-order mean-field approximation, in which the (local) probability that neighbors of the motif are excited is given by the (global) steady-state mean-field excitation density c_E^*.

This general idea of mean-field for embedded devices is specially fruitful when considering the contribution of cycles (i.e. closed paths) to the overall dynamical behavior. Indeed, cycles are a feature not accounted in standard nor even in refined (pair-correlations or degree-classes) mean-field approaches, while they play a key role in excitable dynamics by contributing to excitation amplification and sustained activity [13, 12, 11]. In the case of an absolute excitation threshold $q = 1$, we detail below in § 4.2 how to compute

the average success rate of a cycle, by considering that it is embedded in a mean-field environment. We also sketch below in § 4.3 the application of this methodology to study co-activation, by using a shell model around a hub [17].

4.2. Excitation of a cycle

In a cycle of length L (i.e. a closed path of L nodes), a cycling excitation vanishes as soon as it meets a refractory node. Only long cycles can persistently store excitation: cycles should be long enough so that excitation always faces a susceptible substrate. Quantitatively, the probability π_L that a site R as recovered after $L-2$ steps, in time to accommodate the cycling excitation, should be close enough to 1. The simple computation (ignoring correlations with the surroundings) yields $\pi_L = \sum_{j=0}^{L-3}(1-p)^j p = 1-(1-p)^{L-2}$. Failure of re-excitation thus occurs on average after a time

$$\tau_{break}(p,L) = \frac{1}{(1-\pi_L)} = \frac{1}{(1-p)^{L-2}} \tag{4.1}$$

The quantity $\tau(L,p) = L-1+\tau_{break}(p,L)$ provides an estimate of the average runtime of the cycle. Using a similar reasoning, the probability that there is exactly N re-excited nodes in a row in the cycle is $\pi_L^N(1-\pi_L)$. The time after which failure of re-excitation occurs thus follows exactly a geometric distribution with parameter $1-\pi_L$. Accordingly, the corresponding variance, which coincides with the variance of the cycle runtime, is equal to $\pi_L/(1-\pi_L)^2$. In particular, $\pi_L = p$ for a triangle ($L=3$), and the runtime is predicted to be equal to $2+1/(1-p)$ with a standard deviation $\sqrt{p/(1-p)^2}$. The good accuracy of this simple analysis is shown on Fig. 5.

A more detailed analysis shows that a cycle that is initially all susceptible and receives an excitation does not trigger a cycling excitation. It should also contain a refractory node, otherwise two waves of excitation will propagate in opposite direction and ultimately annihilate, which does not correspond to a cycling excitation. The probability that excitation of a cycle sets in is thus difficult to compute, as it essentially depends on the initial condition of the cycle. This difficulty has been circumvented above by computing the number of re-excitations N_{reex}, defined as the number of excitations following in a row the completion of a cycle. $N_{reex} = 1$ if the cycle excitation only closes onto itself, $N_{reex} = L+1$ if a second full turn is completed. N_{reex} is a number that is not a multiple of L in case of incomplete turns.

We can provide a refined estimate of the probability of continued excitation of a cycle, i.e. re-excitation of its nodes, using the second-order mean-field methodology described above. For simplicity we consider the case with no spontaneous excitations ($f=0$). To get re-excited nodes, we have to consider that they do not fail to recover in time, and once recovered, that they do not receive a perturbing external excitations. Considering all the possible timings j between 1 and $L-2$ steps for the recovery, and the subsequent absence of external inputs during the $L-2-j$ remaining steps, we obtain

the probability $\gamma(L,p)$ of a re-excitation:

$$\begin{aligned}\gamma(L,p) &= \sum_{j=1}^{L-2} p(1-p)^{j-1}[(1-c_E^*)^{\langle k\rangle-2}]^{L-2-j} \\ &= p \times \frac{[(1-c_E^*)^{\langle k\rangle-2}]^{L-2}-(1-p)^{L-2}}{(1-c_E^*)^{\langle k\rangle-2}-(1-p)} \end{aligned} \tag{4.2}$$

Note that for a triangle, $L=3$, the sum (correctly) contains a single term, yielding $\gamma(L,p)=p$: there is no way to perturb a cycling excitation along a triangle ESR except by a lack of recovery, the effect of which is analyzed in Fig. 5.. In this mean-field approach, $\gamma(L,p)^N$ is the cumulative probability to have at least N re-excitations in a row, while the probability to have exactly N re-excitations in a row is $(1-\gamma(L,p))\gamma(L,p)^N$. The average number of re-excitations following cycle completion becomes:

$$\langle N_{reex}\rangle = \frac{\gamma(L,p)}{1-\gamma(L,p)} = \tau_{break}-1 \tag{4.3}$$

In particular, (4.1) is recovered for a triangle, with $L=3$ and $\gamma(L,p)=p$. Under the assumption that re-excitations dominate cycle activity, i.e. the cycle completion is followed by several turns of cycling re-excitation, this mean-field computation also gives the probability that at a given time a L-cycle is active, equal to $\gamma(L,p)^L$. The computation (4.2) involves several mean-field approximations: the probability of excitation of a cycle neighbor is taken equal to the steady-state mean-field excitation density c_E^*, the correlations between the states of the cycle neighbors are ignored, and the degree of cycle nodes are replaced by the average degree $\langle k\rangle$. This latter approximation could be eliminated by considering explicitly the degrees $(k_1,\ldots,k_L)$ of the cycle nodes. The probability of N re-excitations following cycle completion is then given by:

$$P(N,L,p) = \prod_{\alpha=1}^{N}\left[\sum_{j=1}^{L-2} p(1-p)^{j-1}[(1-c_E^*)^{k_\alpha-2}]^{L-2-j}\right] \tag{4.4}$$

where the label α of the degree should be understood modulo L, starting from the node having received the excitation. If another excitation enters the cycle at some susceptible node before the cycling excitation arrives, a phase slip is observed [12].

4.3. Shell model of hub-induced co-activation

In the case of an excitable dynamics with an absolute threshold $q=1$, the qualitative analysis of the dynamics suggests that hubs act as sources of excitation, spreading any single excitation they have received from their numerous neighbors. To quantitatively check whether this phenomenon actually dominates the dynamics, we considered the graph as a set of nested shells centered on the strongest hub [17]. Nodes belonging to the same shell are by definition at the same distance to the hub (Fig. 6). We first estimate the

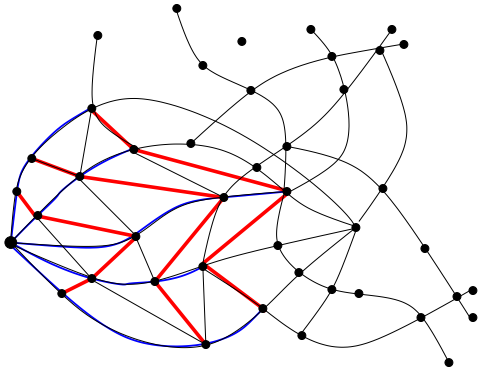

FIGURE 6. **Shell model for analytical estimation of co-activation.** When the graph has a broad degree distribution, the excitable dynamics with an absolute threshold $q = 1$ is presumably dominated by the presence of hubs. We thus propose to represent the graph as a nested set of shells (bold red) centered around the strongest hub. Co-activation is then approximated as the synchronous activation of nodes in the same shell by an excitation propagating from the hub

probability of excitation of the hub, of degree k_{hub}, by identifying it with the mean-field excitation density c_E^* for an average degree $\langle k \rangle = k_{hub}$, given in (2.2):

$$c_E(hub) = c_E^*(k_{hub}) \tag{4.5}$$

Comparison of this prediction and numerical simulation for hubs of various degrees is shown on Fig. fig:MF-hub, as a function of their degree k_{hub}.

Once the hub gets excited, nodes of the same shell will be reached at the same time by the excitation wave propagating from the hub. Accordingly, they will get excited jointly provided they are both in a susceptible state when the excitation wave arrives. The probability of such an event for a given pair of nodes, presumed to be the main contribution to the probability of their co-activation, can be computed in the mean-field approximation. We have to express that each node of the two paths from the hub to the considered nodes is susceptible when the excitation wave arrives. When ignoring pair correlations, the co-activation probability of any given pair of nodes in shell n can be written:

$$Q_n = c_{hub}^*(E)[c^*(S)]^{2n} \tag{4.6}$$

The comparison of this analytical prediction with the co-activation probability observed in the simulation has shown that excitations are more strongly coordinated in space and time than accounted in the derivation of (4.6). Dynamic correlations between neighbors should also be taken into account,

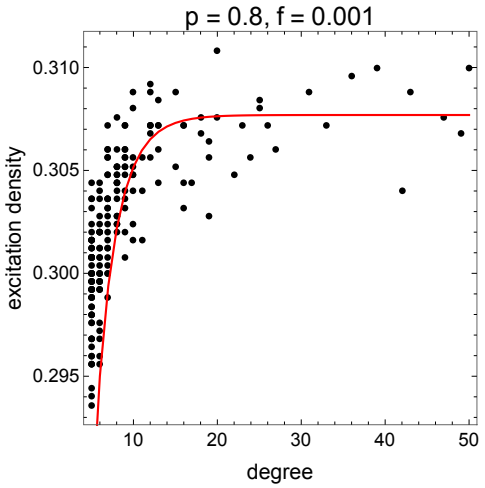

FIGURE 7. **Prediction of the steady-state excitation density of a node as a function of its degree.** The figure compares the prediction (4.5), red line, and the simulation result for various nodes (scatter plot, black dots). The simulation has been performed for the excitable model with an absolute threshold $q = 1$, with $p = 0.8$ and $f = 0.001$, on a scale-free graph (Barabási-Albert) with 100 nodes and 985 links (corresponding to $m = 5$ links being added per node during preferential attachment).

for instance using the pair-correlation mean-field equations detailed above in § 2.5, see [17] for details.

5. Conclusion

Mean-field approaches provide an analytical way to get some insights on excitable dynamics on graphs. They involve a closure relation, namely they ignore some correlations, and some kind of spatial homogenization, namely they also ignore most spatial structures and heterogeneities. Sometimes, a self-consistent validity check is possible. However, we claim that the most interesting insights come from either the agreement or the discrepancies between mean-field predictions and what is observed in numerical experiments. In this regard, analytical approaches are used as null models, as a way of hypothesis testing, to check the validity of their assumptions by comparing their predictions with direct simulation. Mean-field approaches presented above thus offer a sequence of nested null models, increasingly taking into account graph topological features.

Our previous and present investigations have shown that the validity and accuracy of mean-field approaches strongly depend on the observable. They are in general satisfactory for describing excitation density, but of more limited validity for investigating complex features like co-activation or sustained activity. Mean-field failure reveals the presence and key role of collective patterns of activity. When these collective patterns are rooted in some topological motifs, we propose a methodology based on mean-field-embedded devices, that is, the detailed description of the activity of a subset of nodes, given that their surrounding is described by mean-field densities. Beyond the examples detailed above for excitable dynamics with an absolute threshold $q = 1$, we also successfully implemented this mean-field methodology in the case of a relative excitation threshold, for instance to compute the contribution of multiple excitations meeting at a node and increasing the probability that this node gets excited and propagates the excitation [11]. This original methodology circumvents the limitation coming from the spatial homogenization involved in more basic mean-field approaches, and provides an analytical access to the interplay between dynamics and the underlying network topology. Joining these analytical results and simulation at the same time validates our analytical understanding and guides the interpretation of the detailed numerical results.

Mean-field approaches can be applied to a variety of other dynamical processes on graphs. What we have described using the formalism of graphs and excitable dynamics can be extended to numerous other settings, for instance reaction-diffusion on a structured substrate, in surface chemistry, or colonization-extinction processes on a heterogeneous landscape, in ecology.

Acknowledgment

The authors warmly thank Delio Mugnolo, Fatihcan Atay and Pavel Kurasov, organizers of the ZiF programme *Discrete and continuous models in the theory of networks*, and ZiF (Center for Interdisciplinary Research) in Bielefeld for hospitality during this programme. This work was also funded by the French Centre National de la Recherche Scientifique (CNRS), programme InFIniTI of the Mission for Interdisciplinarity, grant 238301 (to A.L.).

References

[1] Barabasi, A., and Albert, R. Emergence of scaling in random networks. *Science 286*, 5439 (1999), 509.

[2] Barrat, A., Barthelemy, M., and Vespignani, A. *Dynamical processes on complex networks*. Cambridge University Press, 2008.

[3] Barthélemy, M. Spatial networks. *Physics Reports 499*, 1-3 (2011), 1–101.

[4] Barthelemy, M., Barrat, A., Pastor-Satorras, R., and Vespignani, A. Dynamical patterns of epidemic outbreaks in complex heterogeneous networks. *Journal of Theoretical Biology 235*, 2 (2005), 275–288.

[5] Boccaletti, S., Latora, V., Moreno, Y., Chavez, M., and Hwang, D. Complex networks: Structure and dynamics. *Physics Reports 424*, 4 (2006), 175–308.

[6] Carvunis, A., Latapy, M., Lesne, A., Magnien, C., and Pezard, L. Dynamics of three-state excitable units on Poisson vs. power-law random networks. *Physica A: Statistical Mechanics and its Applications* (2006).

[7] Catanzaro, M., Boguñá, M., and Pastor-Satorras, R. Diffusion-annihilation processes in complex networks. *Physical Review E 71*, 5 (2005), 056104.

[8] Christensen, K., Flyvbjerg, H., and Olami, Z. Self-organized critical forest-fire model: Mean-field theory and simulation results in 1 to 6 dimenisons. *Physical Review Letters 71*, 17 (1993), 2737.

[9] Dangerfield, C., Ross, J., and Keeling, M. Integrating stochasticity and network structure into an epidemic model. *Journal of the Royal Society Interface 6*, 38 (2009), 761–774.

[10] Erdös, P., and Rényi, A. On random graphs, i. *Publicationes Mathematicae (Debrecen) 6* (1959), 290–297.

[11] Fretter, C., Lesne, A., Hilgetag, C. C., and Hütt, M.-T. Topological determinants of self-sustained activity in a simple model of excitable dynamics on graphs. *Scientific reports 7* (2017), 42340.

[12] Garcia, G. C., Lesne, A., Hilgetag, C. C., and Hütt, M.-T. Role of long cycles in excitable dynamics on graphs. *Physical Review E 90*, 5 (2014), 052805.

[13] Garcia, G. C., Lesne, A., Hütt, M., and Hilgetag, C. C. Building blocks of self-sustained activity in a simple deterministic model of excitable neural networks. *Frontiers in Computational Neuroscience 6* (2012), 50.

[14] Gleeson, J. P., Melnik, S., Ward, J. A., Porter, M. A., and Mucha, P. J. Accuracy of mean-field theory for dynamics on real-world networks. *Physical Review E 85*, 2 (2012), 026106.

[15] Graham, I., and Matthai, C. C. Investigation of the forest-fire model on a small-world network. *Physical Review E 68* (2003), 036109.

[16] Hethcote, H. W. Mathematics of infectious diseases. *SIAM Review 42* (2000), 599.

[17] Hütt, M., and Lesne, A. Interplay between topology and dynamics in excitation patterns on hierarchical graphs. *Frontiers in Neuroinformatics 3* (2009).

[18] Hütt, M.-T., Jain, M., Hilgetag, C. C., and Lesne, A. Stochastic resonance in discrete excitable dynamics on graphs. *Chaos, Solitons and Fractals 45* (2012), 611–618.

[19] Landau, L. D., and Lifshitz, E. M. *Statistical physics*. Pergamon Press, London, 1958.

[20] Lesne, A., and Laguës, M. *Scale invariance: From phase transitions to turbulence*. Springer, Paris, 2011.

[21] Müller-Linow, M., Marr, C., and Hütt, M. Topology regulates the distribution pattern of excitations in excitable dynamics on graphs. *Physical Review E 74*, 1 (July 2006), 1–7.

[22] Murrell, D. J., Dieckmann, U., and Law, R. On moment closures for population dynamics in continuous space. *Journal of theoretical biology 229*, 3 (2004), 421–432.

[23] Pastor-Satorras, R., and Vespignani, A. Epidemic spreading in scale-free networks. *Physical Review Letters 86* (2001), 3200–3203.

[24] Roy, M., and Pascual, M. On representing network heterogeneities in the incidence rate of simple epidemic models. *Ecological Complexity 3*, 1 (2006), 80–90.

[25] Simoes, M., da Gama, M. T., and Nunes, A. Stochastic fluctuations in epidemics on networks. *Journal of The Royal Society Interface 5*, 22 (2008), 555–566.

[26] Vazquez, F., and Eguíluz, V. M. Analytical solution of the voter model on uncorrelated networks. *New Journal of Physics 10*, 6 (2008), 063011.

[27] Weber, S., and Porto, M. Multicomponent reaction-diffusion processes on complex networks. *Physical Review E 74*, 4 (2006), 046108.

[28] Weiss, P. La variation du ferromagnétisme avec la température [in French]. *Comptes Rendus 143* (1906), 1136–1139.

Marc-Thorsten Hütt
Department of Life Sciences and Chemistry
Jacobs University Bremen
D-28759 Bremen
Germany
e-mail: `m.huett@jacobs-university.de`

Annick Lesne
Sorbonne Université, CNRS,
Laboratoire de Physique Théorique de la Matière Condensée
F-75252, Paris
France
& Institut de Génétique Moléculaire de Montpellier
University of Montpellier, CNRS
F-34293, Montpellier
France
e-mail: `lesne@lptmc.jussieu.fr`